Three-Dimensional Image Reconstruction of Insect Flight Muscle. I. The Rigor Myac Layer

K. A. Taylor, M. C. Reedy, L. Córdova, and M. K. Reedy

The Department of Cell Biology, Duke University Medical Center, Durham, North Carolina 27710-3011

Abstract. We have obtained detailed three-dimensional images of in situ cross-bridge structure in insect flight muscle by electron microscopy of multiple tilt views of single filament layers in ultrathin sections, supplemented with data from thick sections. In this report, we describe the images obtained of the myac layer, a 25-nm longitudinal section containing a single layer of alternating myosin and actin filaments. The reconstruction reveals averaged rigor cross-bridges that clearly separate into two classes constituting lead and rear chevrons within each 38.7-nm axial repeat. These two classes differ in tilt angle, size and shape, density, and slew. This new reconstruction confirms our earlier interpretation of the lead bridge as a two-headed cross-bridge and the rear bridge as a single-headed cross-bridge. The importance of complementing tilt series with additional projections outside the goniometer tilt range is demonstrated by comparison with our earlier myac layer reconstruction. Incorporation of this additional data reveals new details of rigor cross-bridge structure in situ which include clear delineation of (*a*) a triangular shape for the lead bridge, (*b*) a smaller size for the rear bridge, and (*c*) density continuity across the thin filament in the lead bridge. Within actin's regular 38.7-nm helical repeat, local twist variations in the thin filament that correlate with the two cross-bridge classes persist in this new reconstruction. These observations show that in situ rigor cross-bridges are not uniform, and suggest three different myosin head conformations in rigor.

MUSCLE contraction is believed to be due to the active sliding motion of interdigitating sets of thick, myosin-containing filaments and thin, actin-containing filaments (Huxley and Neidergerke, 1954; Huxley and Hanson, 1954). The sliding motion is generally thought to be produced by the ATP-driven cyclical attachment of myosin cross-bridges to the thin filaments (Huxley, 1957). While the sliding filament model has found wide support, there are many structural details accompanying tension generation that have still to be determined. The most widely held theory (Huxley, 1969) was prompted in part by electron microscopic images of insect flight muscle (IFM)[1] in the relaxed and rigor states (Reedy et al., 1965). This theory holds that the detached 90° cross-bridges observed in relaxed muscle tilt to 45° after attachment to actin, thus accounting for the tension that accompanies rigor induction and suggesting a general model for tension development in active muscle. According to this model, rigor cross-bridges exhibit the end of the power stroke and therefore justify detailed study.

Cross-bridges in situ can be seen to best advantage in the highly ordered lattice of the flight muscle of the large water bug *Lethocerus*. However, IFM differs from the more widely studied vertebrate striated muscle in several respects. In *Lethocerus* the actin filaments are located midway between pairs of thick filaments. Thus, cross-bridges form attachments only between actin filaments and their two nearest-neighbor thick filaments. *Lethocerus* thick filaments contain four myosin molecules per 14.5-nm axial period (Reedy et al., 1981) rather than the three found in thick filaments of vertebrate striated muscle (Tregear and Squire, 1973; Lamvik, 1978; Kensler and Stewart, 1983). Recently, direct evidence (Reedy, M. C., A. D. Magid, and M. K. Reedy, manuscript submitted for publication) has been shown for four start helical tracks on isolated *Lethocerus* thick filaments with an axial spacing of 38.7 nm (Wray, 1979), a value identical to that of the long-pitch helices of the thin filament and clearly different from the 42.9-nm myosin repeat of vertebrate thick filaments. *Lethocerus* also contains a heavy troponin complex of MW 168 kD (Bullard et al., 1988) that is twice as large as vertebrate troponin. Despite these differences in filament arrangement and molecular organization, we expect that general concepts pertaining to cross-bridge structure can be determined from the particulars of IFM.

Our previous studies of IFM have revealed two forms of rigor cross-bridge of strikingly different structure (Taylor et al., 1984; Reedy and Reedy, 1985). One of these appeared tilted at a 45° angle but was backbent from the slew curvature observed in acto-S1. The other was much less tilted but showed conventional S1 slew curvature. The size of both forms seemed large enough to contain two myosin heads but density differences suggested that on average one form con-

1. *Abbreviations used in this paper*: Acto-HMM, complex between F actin and HMM; acto-S1, complex between F actin and S1; HMM, heavy meromyosin; IFM, insect (fibrillar) flight muscle; S1, myosin subfragment-1; 3-D, three dimensional.

© The Rockefeller University Press, 0021-9525/89/09/1085/18 $2.00

tained two myosin heads while the other contained one delocalized head. Our three-dimensional (3-D) reconstruction also suggested that both heads of a myosin molecule bind along a single thin filament and furthermore, that actin filament twist was locally perturbed in regions where cross-bridges bind. We concluded that the end of the power stroke in rigor IFM encompassed two crossbridge conformations.

In this communication we reexamine the structure of the rigor myac layer deduced through 3-D image reconstruction, by considering the effect of additional data obtained from thick sections on our earlier reconstruction from tilt series. This additional data fills out the equatorial and meridional planes of the transform thereby completing important regions of data that were missing in our earlier work. New details of the shape and distribution of rigor cross-bridges and their interaction with the thin filament are revealed in this reconstruction. Not only do we confirm different cross-bridge angles but we can infer that individual heads of double-headed cross-bridges may have different conformations.

Materials and Methods

Specimen Preparation

Dorsal longitudinal flight muscle of *Lethocerus indicus* was glycerinated in situ in the thorax (Reedy et al., 1981). Fiber bundles were mounted in an x-ray cell and stretched 2–3% above slack length to insure good orientation. Fibers were fixed using 0.2% tannic-acid with 2.5% glutaraldehyde, followed by cold 1% OsO_4 at pH 6.0. Tissue was block stained with 2% uranyl acetate, embedded in Araldite 506-DDSA and sectioned as described previously (Reedy et al., 1983; Reedy and Reedy, 1985). Sections were stained with the permanganate-lead sequence. Preparation was documented by x-ray diffraction before and after fixation and embedding (Reedy and Reedy, 1985). All sections were obtained from the x-ray monitored specimen bundle No. 958. The thick filament spacing determined by x-ray diffraction of the fixed-embedded bundle was 52 nm (Reedy and Reedy, 1985). Note that section compression reduces the interfilament spacing in myac layers to 46.6 nm.

Electron Microscopy

For practical reasons, survey of sections and collection of tilt series data in the electron microscope was carried out without resorting to minimal dose techniques; therefore the selected area accumulated a high electron dose. Radiation damage results in specimen thinning (Bennett, 1974; Berriman and Leonard, 1986), most of which occurs in the first few seconds of observation (Egerton, 1980), so that specimen thickness has essentially stabilized before collection of tilt series data. Nevertheless, to minimize the effects of any further section thinning on the reconstruction, our protocol was to record high tilt angles first. Two tilt series were recorded at intervals of 10°, one taken with the tilt axis parallel to the filament axis and the other with it perpendicular to the filament axis. Tilt series data were collected on a Philips EM400 electron microscope operated at 80 kV. Thick section images were collected on a Philips EM300 electron microscope also operated at 80 kV.

Image Analysis

The reconstruction was done by combining merged tilt series data from the myac layer thin section with projection data obtained from a thick transverse and a thick longitudinal section. The procedure is an adaptation of that first used in reconstructions of two-dimensional crystalline arrays (Amos and Baker, 1979). The reconstruction scheme, illustrated in Fig. 1, provides three orthogonal views of the myac layer in addition to those views provided by the tilted thin section. Microtomy, in effect, "windows" the myac layer from the 3-D filament lattice. Views orthogonal to the plane of the myac layer are obtained from appropriately windowed regions of the thick section images.

The myac layer tilt series images were digitized on the densitometer at the MRC Laboratory of Molecular Biology (Cambridge, UK) in 1981. Myac row and myac column data were digitized at a later date than the tilt series data on a microdensitometer (model 1010M; Perkin-Elmer Corp., Pomona, CA) linked to an LSI 11/23 host computer. Densitometer step sizes with respect to the original object were 1.0 nm for the thick transverse section image, 1.2 nm for the thick longitudinal section image, and 1.7 nm for the myac layer images (the latter two determined based on internal calibration using a spacing of 38.67 nm for the third order of the fundamental axial period of 116 nm).

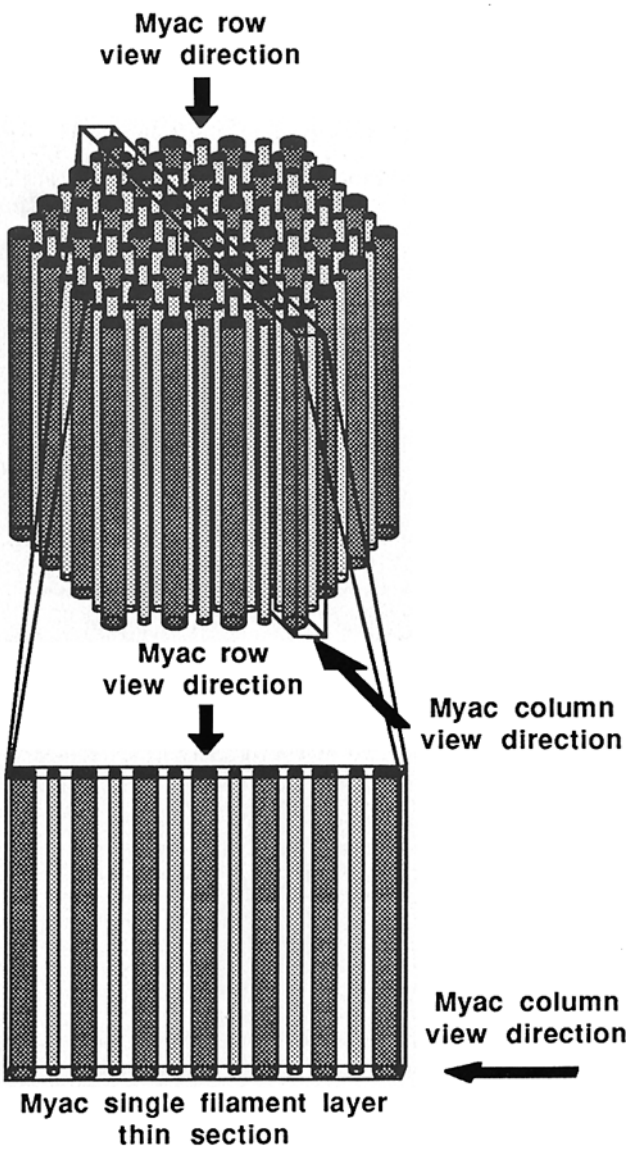

Figure 1. Diagram illustrating the relationship between the views of the myac layer derived from thick sections and the myac layer itself. Myac layers are found in 25-nm longitudinal sections cut parallel to the 10.0 planes of the hexagonal filament lattice. They contain alternating thick and thin filaments. The physical sectioning process is akin to windowing the myac layer from the 3-D filament lattice. "Myac rows" are rows of alternating thick and thin filaments windowed from images of thick transverse sections viewed down the 00.1 direction and are equivalent to myac layers tilted 90° about an axis perpendicular to the filament axis. Their Fourier transform provides a complete equatorial plane of the myac layer transform. "Myac columns" are windowed from images of thick longitudinal sections viewed down the 10.0 planes and are equivalent to myac layers tilted 90° about an axis parallel to the filament axis. The Fourier transform of a myac column provides a complete meridional plane of the myac layer transform.

Analysis of the tilt series electron micrographs was carried out essentially as described previously (Taylor et al., 1984). The calculated transform was sampled on an axial 116-nm period, the smallest repeat containing integral multiples of the 14.5-nm-thick filament and the 38.7-nm-thin filament periods. The phase origin refinement and merging steps were carried out initially in space group p12 (nomenclature of Holser [1958]), in which twofold rotation axes are presumed coincident with both thick and thin filament axes. To obtain a reconstruction without enforced symmetry, the tilt series data were merged in the two-sided plane group p1 using the origin shifts and amplitude scaling determined for the p12 reconstruction. The data were then subjected to several cycles of origin refinement and amplitude scaling in p1 to give the data opportunity to find a different minimum. This procedure was done both for convenience and to insure that the origin of the p1 map was close to the presumptive twofold axis of the filaments. The quality of fit was similar in both cases, although slightly better when no symmetry is assumed, i.e., in p1. Origin shifts between p12 and p1 were <2° for all but one image. In general, the quality of transform data falling on the 3rd, 6th, 8th, and 9th orders of the 116-nm axial period was noticeably superior to the other nonequatorial lattice lines. The merged tilt series data were fitted by a least squares procedure that assumed a specimen thickness of 25 nm. This fitting procedure is not particularly sensitive to the section thickness, within physically reasonable limits.

Myac rows and myac columns were processed by first interpolating the images themselves to correct for rotational misalignment with the sampling grid and to insure that an integral number of unit cells were contained within each output image array. In addition, each image was subjected to gaussian edge apodization before Fourier transformation. The procedure is similar to that used by Kensler and Stewart (1983) in Fourier-Bessel 3-D image reconstructions of thick filaments. It differs from that described earlier for the myac reconstruction in which correction for image rotation was carried out by interpolation in reciprocal space (Taylor et al., 1986) without edge apodization. The major effect of the edge apodization is to remove the pronounced edge effects present in the computed transforms, especially those of myac rows, when floating alone is used. 10 equatorial and 9 meridional lattice lines in addition to the (0,0) lattice line were obtained, sampled at intervals of 0.01 nm^{-1}.

Four myac rows and three myac columns were used to calculate averaged data sets for addition to the tilt series data. Averaged myac row and myac column lattice line data were obtained by cross-correlation using programs which in addition to searching for the best origin shift, also allowed for changes in Z^* scaling (which corrects for differences in magnification and other variations between filaments). In principle no changes in Z^* scaling should be necessary since all four myac rows came from the same micrograph of the thick transverse section and all three myac columns came from the same micrograph of the thick longitudinal section. However, slightly better fits could be obtained with scale factors of no more than 5%. To a resolution in Z^* of ~0.2 nm^{-1}, there was good agreement among the four myac row data sets processed for all of the equatorial lattice lines with the exception of the (7,0) and (9,0) lattice lines. Those are not generally observed in myac layer transforms and their absence from the myac row data indicates that the molecular transform in those regions is weak. The (10,0) lattice line was absent in the myac layer tilt series data but was sufficiently reproducible in the myac row transforms to warrant its inclusion in the reconstruction. However, its inclusion caused little change in the reconstruction. Among the three myac column data sets, there was good agreement for only the lattice lines falling on the 0, 3rd, 6th, 8th, and 9th orders of the 116-nm meridional period. The myac column data were particularly difficult to process because of the generally low signal to noise ratio in all but the equatorial lattice line. Presumably this arises from the low contrast of the thin filament and crossbridge features in the image due to their superposition on the dense thick filament. Lattice line data at Z^* resolutions exceeding 0.2 nm^{-1} were generally of low quality. The quality of fit as measured by the phase residuals relative to their respective average was 21° for the myac row data (range 16°-30°) and 33° for the myac column data (range 22°-50°).

The averaged myac row and myac column lattice line data were then cross-correlated with lattice lines fitted to the merged and refined data from the myac layer tilt series. The myac row was fitted to the equatorial lattice lines and the myac column data was fitted to the meridional lattice lines. The averaged myac row lattice line data had to be amplitude scaled and stretched by a factor of 1.6 along Z^* (the transform direction normal to the section plane) before adding it to the previously merged and refined myac layer data obtained from the tilt series. This alignment, which was calculated for all four possible relative orientations, yielded in the best case an amplitude weighted phase residual of 37°. Good correspondence was observed for the lattice lines except the weak (7,0). For the myac column data,

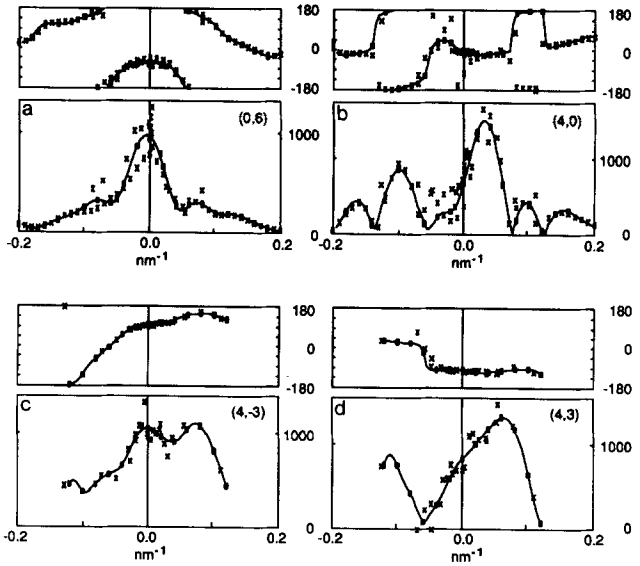

Figure 2. Selected lattice lines used in the reconstruction. Upper diagrams show phases (degrees), lower diagrams amplitude (arbitrary units). (*a*) Meridional (0,6) at an axial spacing of 19.3 nm. (*b*) Equatorial (4,0) lattice line at a spacing of 11.66 nm. *c* and *d* are symmetry related off-meridional lattice lines at a spacing of 11.1 nm. For perfect twofold rotational symmetry about the meridional axis, the phase profile of *d* is related to that of *c* by the relationship: phase (4,3,Z*) = − phase (4,−3,Z*).

a similar procedure was carried out with the result that the best Z^* scaling factor was 1.5 and the phase residual, using just the 3rd, 6th, 8th, and 9th orders of the 116-nm period, was 40°. It is worth noting that the approximate twofold symmetry was also clear in the myac row data because phase residuals showed only slight differences with 180° rotations about the filament axis. The overall agreement between the myac row and the myac column data with the merged tilt series data was better with respect to phases than with respect to amplitudes (Fig. 2).

All myac column lattice lines were amplitude scaled using a single scale factor before merging with the tilt series data; likewise all myac row data were similarly handled. After merging the myac column, row, and myac layer data, there followed a single cycle of origin refinement and amplitude scaling for the myac layer data alone against this merged data set. Finally, after remerging, smooth curves were fit to each lattice line by a least squares fitting procedure. In this final step a section thickness of 25 nm was assumed and the fitted lattice lines were sampled at 0.02 nm^{-1} intervals for purposes of calculating density maps. There was near mirror symmetry of amplitude and phase profiles for the meridional data (e.g., the [0.6] lattice line) and close approximation with real phases for the equatorial data (e.g., the [4.0] lattice line) as shown in Fig. 2. Such behavior is consistent with the presence of twofold rotation symmetry at low resolution. The final data set contains structure factors extending to a resolution of ~5 nm in Z^* while the resolution within the plane is 7.7 nm in the equatorial direction and 12.9 nm in the axial direction.

Rotational correlation functions were determined by calculating the correlation coefficient, *R*, according to the formula

$$R = \frac{\sum_{i=1}^{n} (d_{1i} - \bar{d}_1)\,(d_{2i} - \bar{d}_2)}{\sqrt{\sum_{i=1}^{n} (d_{1i} - \bar{d}_1)^2 \sum_{i=1}^{n} (d_{2i} - \bar{d}_2)^2}},$$

where d_{1i} is the *i*th density of the reference image, in this case the myac layer thin filament, d_{2i} is the corresponding density of the motif image, in this case the acto-S1 helical projection, $\bar{d}_1$ and $\bar{d}_2$ are the respective mean densities. The summation is over the *n* densities of the image.

Mass loss and section compression are unavoidable experimental factors that affect the section and its reconstruction. Of the two, mass loss is by far the greater effect. In the calculations reported here where the myac layer was compared with helical reconstructions of acto-S1, some compensation

for mass loss was deemed necessary. This compensation was achieved by stretching the reconstruction in the Z direction and was applied with the assumption that mass is lost uniformly throughout the section. The rotational correlation calculations were carried out on maps corrected for different degrees of mass loss to assess the effect of this correction on the results. Displays of the reconstruction are shown both with correction for mass loss (surface displays and cylindrical sections are so compensated) and without correction (none of the contour maps shown are compensated).

Section compression is a relatively smaller effect as judged by the 11% reduction in interfilament spacing. However, no theoretical framework exists to predict the effects of the compression on the mass distribution within the section. Experimentally, comparison of 15–25-nm longitudinal sections cut parallel and perpendicular to the filament axis shows no evidence of shearing or rolling of included thin filaments or any other structures within the sections (Reedy and Reedy, 1985). Because it is a relatively small and poorly understood effect, we deemed it prudent not to attempt to compensate for section compression.

Surface contour displays were calculated using a program written by Dr. Guy Vigers (Vigers et al., 1986) for displays of coated vesicle 3-D reconstructions. Surface images and calculated diffraction patterns were displayed on a LEX-90 (Lexidata Corp., Billerica, MA).

Tilt Angle and Viewing Conventions

The tilt angle convention used here is as described in Fig. 1 of Reedy and Reedy (1985). Longitudinal views of the reconstructions are always oriented with the Z line at the bottom, M line at the top. Transverse views of the reconstruction are always viewed towards the Z line. Z and Z^* denote the real and reciprocal space directions perpendicular to the myac layer plane.

Results

Myac Layer Morphology and Diffraction

Myac layers occur where 20–25-nm longitudinal sections contain only a single layer of alternating thick and thin filaments. In rigor myac layers opposed pairs of cross-bridges form doublets every 38.7 nm along the thin filament, the double chevrons (Reedy, 1968). In each doublet the lead chevron lies closest to the M line of the sarcomere and the rear chevron is positioned nearest the Z line.

The myac layer selected for 3-D reconstruction appears homogeneous over an area of at least 0.5 × 0.5 μm and possess a well-ordered cross-bridge array (Fig. 3). Lead chevrons dominate the image. A noticeable variation in the rear chevron levels is manifest as single or incomplete double chevrons. The optical diffraction pattern is typical of myac layers (Fig. 3, *inset*) and shows sampled diffraction of eight equatorial orders and three meridional orders of the 38.7-nm-thin filament period. In addition, a weak layer line arising from the 14.5-nm myosin filament period is observed. Together the 38.7 and 14.5 nm periods define a long 116-nm axial repeat. Unsampled layer lines at 5.9 and 5.1 nm were not found in diffraction patterns from this myac layer although present in diffraction from other sarcomeres in the same section. Since the reconstruction procedure used was restricted to the sampled diffraction, it could not have used these unsampled layer lines even had they been present.

The thick section images were selected for regions with near-circular thick filament profiles (transverse section) and as little sarcomere "barrel shape" as possible (longitudinal section). In the myac row images, the thick filament profile appears nearly uniform in density (Fig. 4 *a*) with no evidence of the hollow core seen in some preparations. Thin filament profiles are predominantly oval but in some cases have a clear division into two densities. These doublets do not, however, occur with enough regularity to show up in averaged images. Diffraction from myac rows consists of nine lattice lines, extending to the 10th order of the interfilament spacing, that together define the equatorial plane of the myac layer transform (Fig. 4 *a*, *inset*). Strong 2nd order peaks are observed on the (1,0) lattice line that are not accessible to measurement from myac layers due to tilting restrictions in the electron microscope. The (0,0) lattice line consists essentially of only a single inner peak.

In the myac column images (Fig. 4 *b*) the 38.7-nm period is faintly visible due to superposition of the thin filaments and cross-bridges onto the dense thick filament. The typical myac column diffraction consists of five lattice lines indexing on a 116-nm period that together define the meridional plane of the myac layer transform (Fig. 4 *b*, *inset*). The (0,0) lattice line is by far the most intense while the third order at a spacing of 38.7 nm has moderate intensity. The 6th, 8th, and 9th orders are very weak in comparison.

Features of the Myac Layer Reconstruction

The myac layer reconstruction contains density features within a region ~16.5 nm in thickness. This value is 65–80% of both the predicted thickness of the myac layer (based upon the known filament geometry and lattice dimensions of IFM) and the observed thickness of the previous reconstruction obtained from tilt series data alone (Taylor et al., 1984). The low thickness of the reconstruction is consistent with expectations based on the amount of Z^* scaling that was required to fit and merge the three types of data used in the reconstruction. Thinning is presumed to result from radiation-induced mass loss from the section. The greater apparent thickness of the earlier reconstruction from tilt series alone is due to the "missing cone" arising from the limited tilt angle range available (i.e., ±60°). This gives rise to a point spread function that is elongated along Z, thereby broadening features of the reconstruction in that direction (Baumeister et al., 1986).

In longitudinal view the lead and rear bridges represent two classes of rigor cross-bridge which differ with respect to tilt, size, density, and shape. Within the 116-nm period there are three levels of double chevrons. The lead bridges are dense features indicating that they are both regular in arrangement and frequent in occurrence in the rigor lattice. They appear highly angled when viewed in untilted sections

Figure 3. Electron micrograph of the untilted rigor IFM myac layer used for the reconstruction (reconstructed area outlined). Double chevrons repeat axially every 38.7-nm period, with a noticeable variation among the three doublet levels within the 116-nm period. The higher density lead chevrons dominate the cross-bridge lattice, exhibiting a steeper and more uniform angle than the thinner and less angled rear chevrons. The variability within a 116-nm repeat is manifest as single chevrons or incomplete double chevrons. The optical diffraction pattern shows near mirror symmetry indicating that the filament layer is well-centered within the section. Diffraction extends to the 8th equatorial order. Two pronounced nonequatorial layer lines are seen at spacings of the 38.7 and 19.3 nm in addition to the weak meridional spot at 12.9 nm. The 14.5-nm meridional spot is barely visible.

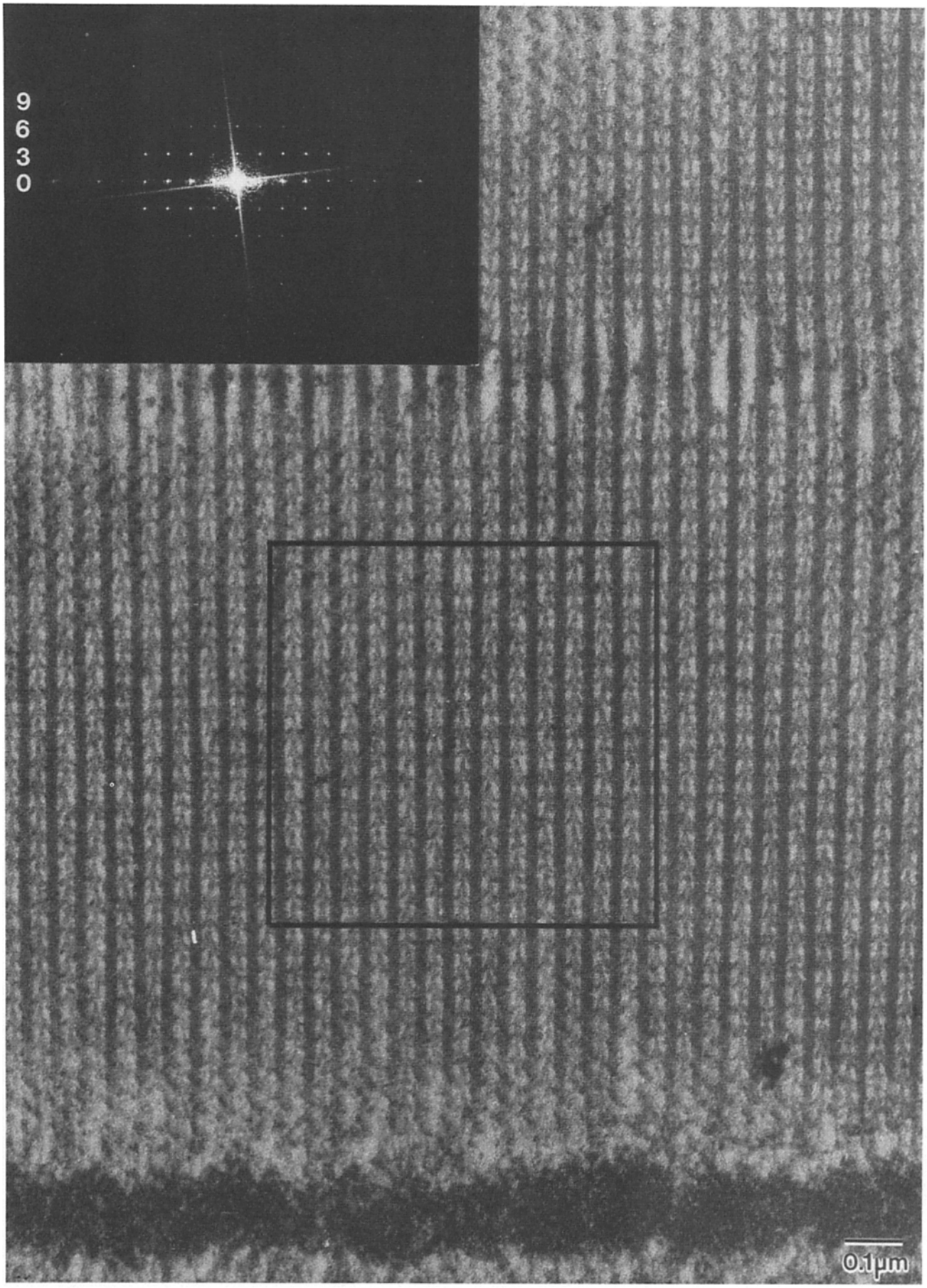
9
6
3
0
0.1μm

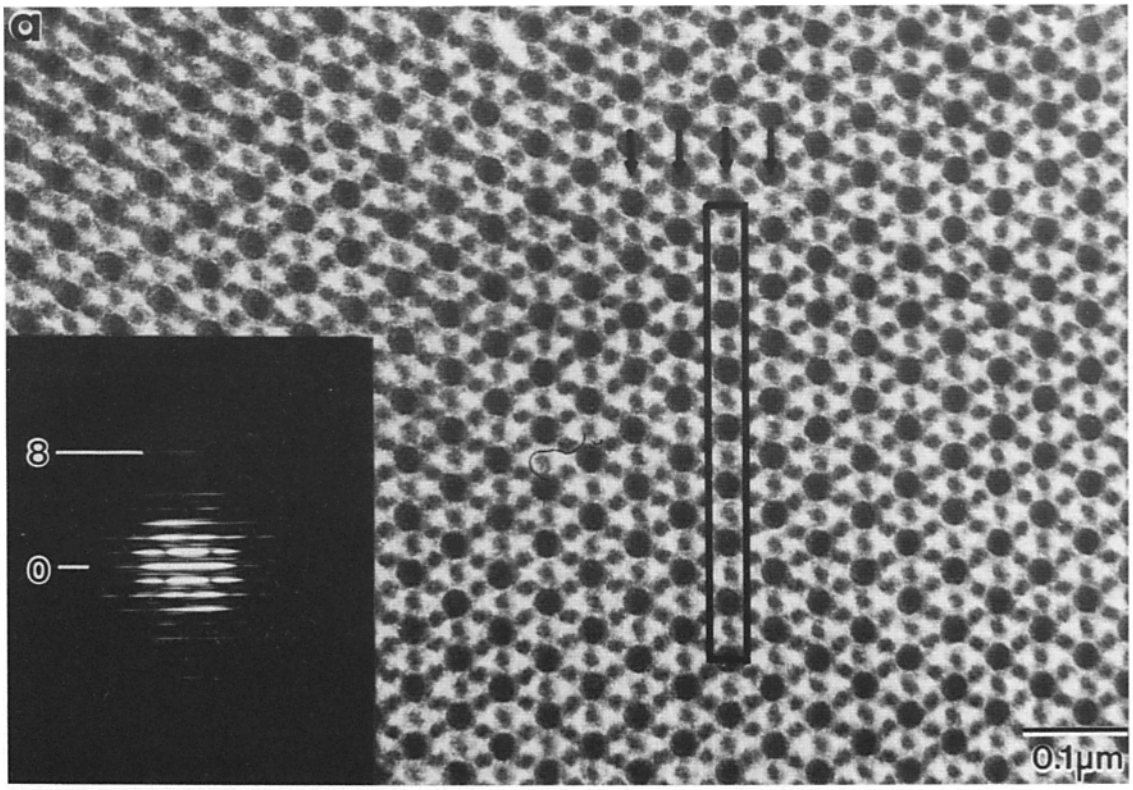
a
8
0
0.1μm

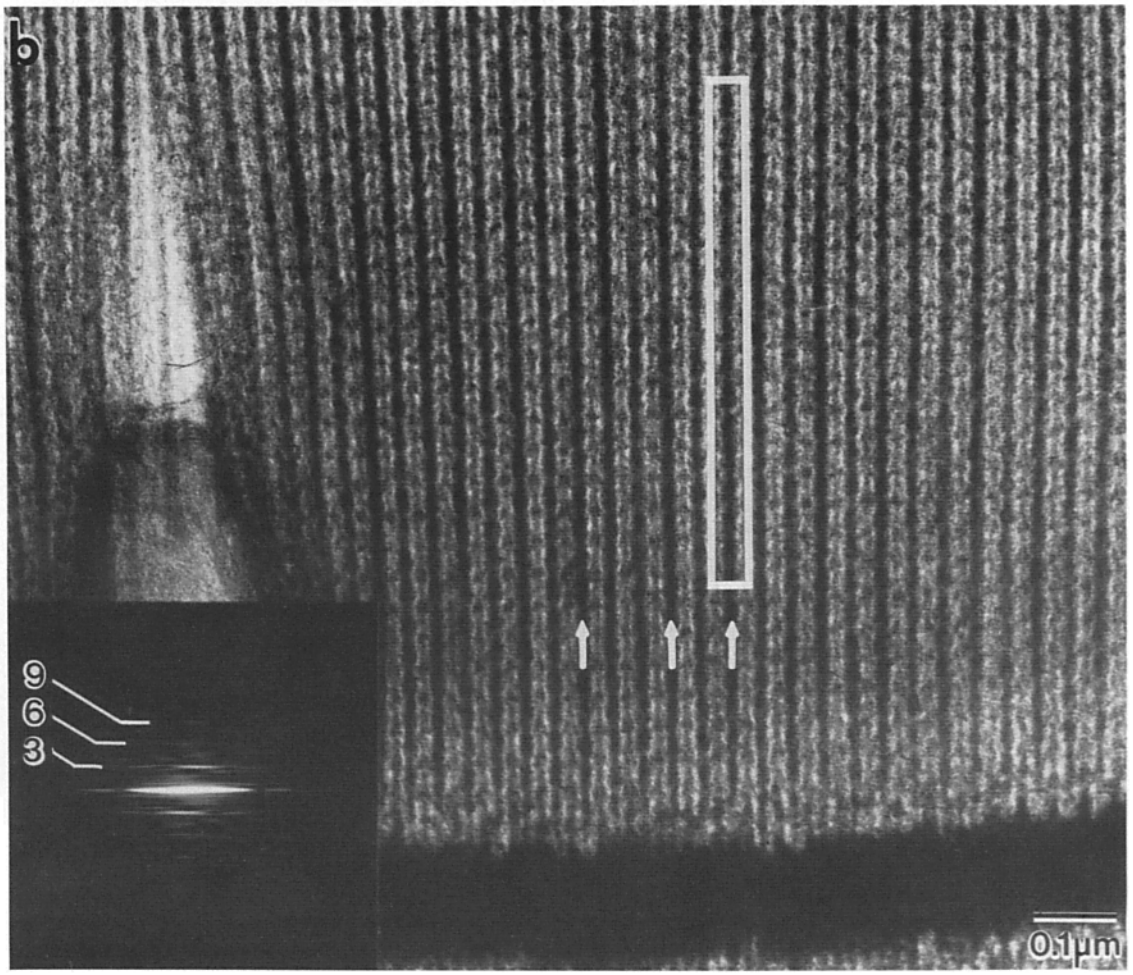
b
9
6
3
0.1μm

(Fig. 5 *b*) and each exhibits a distinctly triangular shape when viewed from a direction about 45° to the interfilament axis (Fig. 5 *a*). One vertex of this triangle contacts the thick filament surface and one edge is located along the thin filament. The forward edge of this triangle (the side closest to the M line) has a length of ~19–20 nm and a slope of 45–50°. The trailing edge (that closest to the Z line) has a length of ~14 nm and is angled nearly perpendicular to the filament axis. The maximum axial extent of lead bridges is 15 nm close to the thin filament. When the reconstruction is viewed in surface representation (Fig. 6), the triangular lead bridge appears rotated relative to the thin filament axis by ~20° (Fig. 6 *c*) in such a way that its trailing edge lies closer to the thick filament surface than the forward edge (see Fig. 12).

The underlying shape of the lead bridge is better illustrated in surface views calculated at a higher contour cutoff (Fig. 7). The lead bridges on one side of the thin filament have a different shape from those on the other side. On one side they deviate slightly from a triangular shape due to the presence of a point of inflection in the forward edge (Fig. 7, *a*, *c*, and *e*, see also Fig. 5 *a*). This point of inflection occurs ~15.0 nm from where we judge the thick filament origin to be and ~4.0 nm from the actin binding site. In acto-S1 reconstructions, a short region of density similar to that observed here projects nearly perpendicular to the thin filament axis before slewing azimuthally and tilting downward toward the 45° angle (Vibert and Craig, 1982; Toyoshima and Wakabayashi, 1985; Milligan and Flicker, 1987; see also Fig. 5 in Amos, 1985). However, the inflection point is much less prominent in the other lead bridge, which has a more triangular profile (Fig. 7, *b*, *d*, and *f*). Both lead bridge shapes are reminiscent of the bound, two-headed structures observed in acto-HMM (Craig et al., 1980). Each of the lead bridges emerges from the thick filament surface as a narrow stem that broadens as it turns tangentially (Fig. 7, *b*, *d*, and *f*). This bent junction between stem and the wider part of the bridge is readily identified as the junction between stem and neck domains described for the flared X by Reedy and Reedy (1985). The triangular shape and size (16 nm) of the lead bridges observed here, the high density of the triangle, and the similarity of the structure to images of acto-HMM all lead to the conclusion that lead bridges are composed of two myosin heads.

In comparison to lead bridges, the rear bridges are smaller, less angled, less dense and show more variation in these properties (Figs. 5 and 6). Variation between the three levels of rear bridge pairs provides the most obvious expression of the 116-nm repeat. At the level where rear bridge size is largest, it is only half that of lead bridges and is shaped more like a bent cylinder than a triangle. One rear bridge at this level appears oriented at 90° while the other is oriented at ~70°. Other rear bridges appear angled between these two values. The gap within the double chevrons naturally depends on the size of lead and rear bridges. This intradoublet gap is typically <5.0 nm, consistent with one unlabeled actin subunit between bridges. Among all three rear bridge levels, density is greater on one side of the thin filament than on the other and greater at one of the axial levels than the other two. The simpler shape and small size (<5 nm) of rear bridges lead to the conclusion that each is composed of a single myosin head.

Several factors affect the size of the averaged cross-bridges in the reconstruction. According to the model of Holmes et al. (1980), the thin filaments are ordered with respect to their pseudo twofold axis in *Lethocerus* flight muscle but may take at random either of the two allowed orientations that differ by 180°. This rotational disorder will lower the averaged density by spreading it axially by ~3 nm, resulting in an overestimate of bridge size. The relative frequency of lead and rear bridges will also affect their average density and therefore their size when displayed at a fixed contour level. Rear bridge positions are less frequently occupied than lead bridge positions so their dimensions are likely to be underestimates. Finally, any buildup of tannic acid on the surface of the cross-bridges would increase the measured size of both lead and rear bridges by the same amount but would affect their relative sizes unequally. However, the substantial differences in size and density between lead and rear bridges exceed any possible effect of the factors just discussed, and strongly support the interpretation that, on average, lead bridges contain two myosin heads while rear bridges contain only one.

In transverse view the bridges have the sigmoidal shape described by Reedy and Reedy (1985) from the flared-X formation seen in single cross-bridge levels in 15-nm cross sections. Lead bridges are more S shaped than rear bridges. The sigmoid is an expression of the tangential myosin contact within the myosin head–actin complex. For purposes of discussion we describe the sigmoid as consisting of two morphological components: a midsegment composed of the paired actin-binding domain of opposite myosin heads with their associated actin monomers, and a neck-stem component at each end that connects the midsegment to the thick filaments. The neck-stem extends tangentially from the midsegment thereby defining the slew curvature of the complex. Thus, the sigmoid contains one midsegment and two neck-stems, comprising a pair of opposed cross-bridges. This terminology is based strictly on shape because the separate domains (i.e., actin, actin-binding domains of myosin, etc.) are not clearly resolved in the reconstruction. It nevertheless has a general parallel with domains implied by the functions of the myosin head. It also differs slightly from the convention used by Reedy and Reedy (1985) in that neck and stem are treated here as a single domain. The chirality of the sigmoid is accounted for solely by the tangentially disposed neck-stems.

The slew of lead and rear bridges differ, in contrast to the uniform slew seen in vitro. Reconstructions of acto-S1 show the portion of the head distal to the actin binding site slewing

Figure 4. Electron micrographs of the thick sections of rigor IFM used in the reconstruction. (*a*) Thick transverse section with one myac row outlined. Arrows indicate other myac rows used in the averaged data. (*b*) Thick longitudinal section with one myac column outlined. Arrows indicate other myac columns used in the averaged data. Computed diffraction patterns of the windowed regions are shown in the insets. The amplitude profiles of the equatorial lattice lines (*inset* in *a*) and the meridional lattice lines (inset in *b*) provide similar information to that given by the amplitude portion of the lattice line plots shown in Fig. 2.

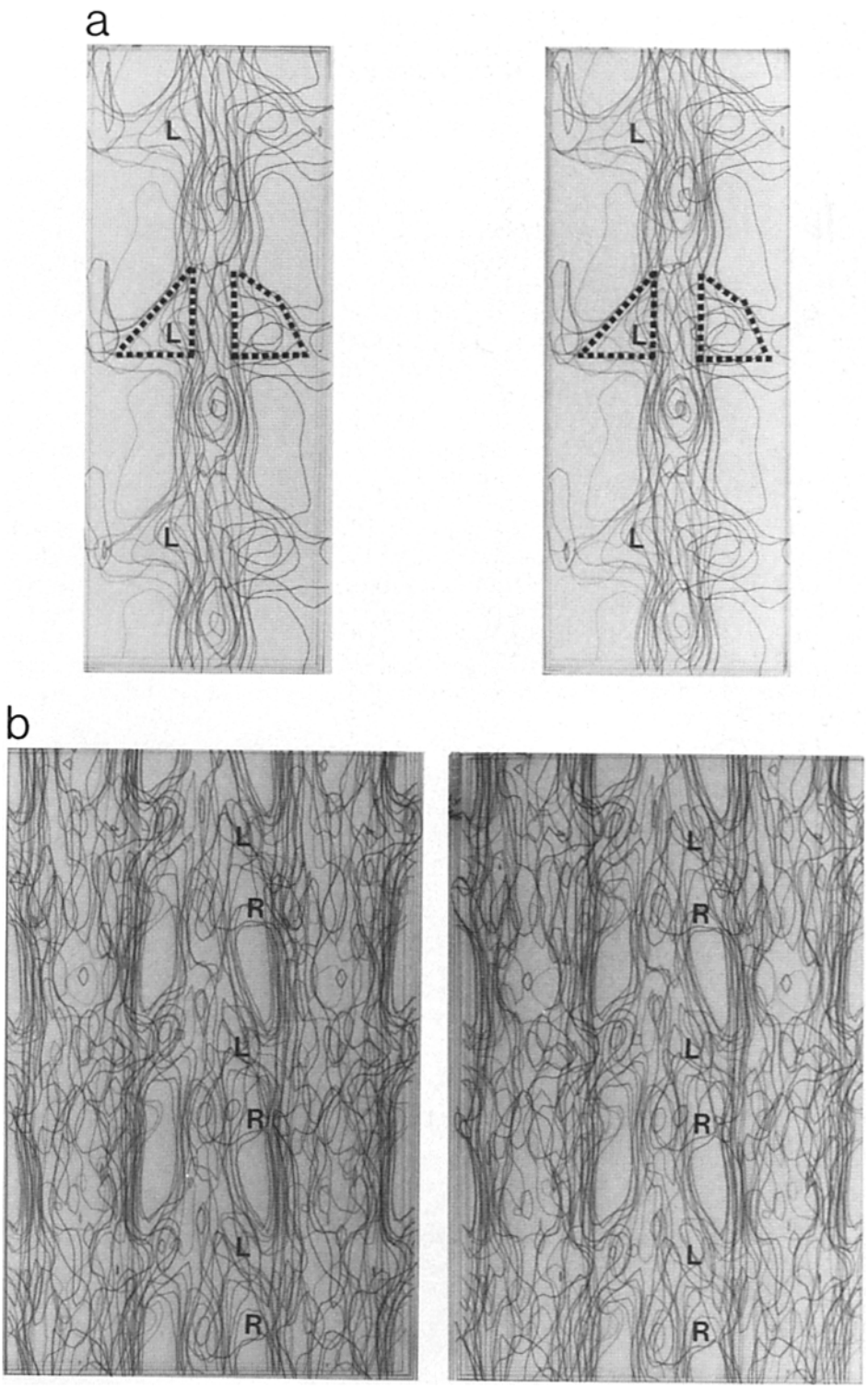

Figure 5. Three-dimensional contour maps of the rigor IFM myac layer. These stereo pairs are from the pl reconstruction. The selection of contour cutoff for display was made such that the rear bridges would be clearly visualized. The axial direction (vertical) contains one 116-nm repeat composed of three pairs of lead and rear bridges. Lead and rear bridges are labeled *L* and *R*, respectively. (*a*) This map was obtained by reinterpolating the reconstruction at an angle of 45° to the interfilament axis to show more clearly the triangular shape of the lead bridge. The direction of view here is from the back left side of the map in *b*. Dashed lines frame lead bridges to illustrate the inflection in the forward edge of some lead bridges. (*b*) This map is equivalent in view direction to an untilted myac layer.

and bending in a single curve around the axis of the thin filament (Moore et al., 1970; Toyoshima and Wakabayashi, 1985; Taylor and Amos, 1981; Vibert and Craig, 1982; Milligan and Flicker, 1987). Rear bridges extend radially from the thick filament surface and curve to their thin filament binding sites with the conventional S1 slew curvature (see Fig. 9, *c* and *d*). Lead briges bend from a narrow stem to lie tangential to the thick filament surface (Fig. 7, *b* and *d*, Fig. 9, *f* and *g*), and contact their midsegment with a more acute angle than the rear bridges. The lead bridge stem does not follow the line of the bridge neck but instead bends backward from the slew curvature established by neck and midsegment.

These differences in slew curvature imply two regions of flexibility. A point of flexibility in myosin near the junction of the two heads is required to account for the disposition of cross-bridges along radial and tangential directions on the thick filament. This point may be identified with the swivel

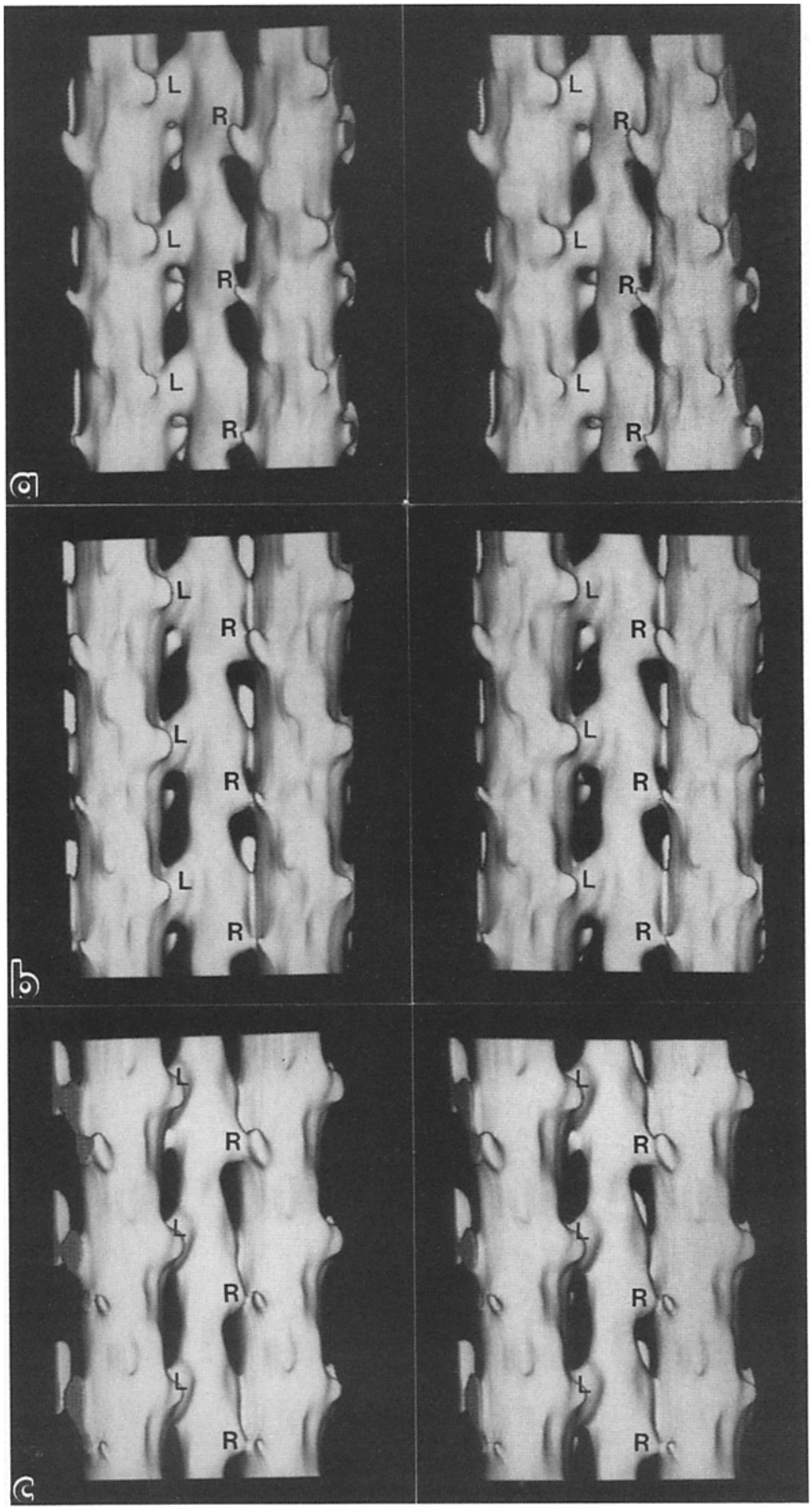

Figure 6. Stereo surface views at different tilt angles of the myac layer reconstruction done in the two-sided plane group p1. These three views correspond in orientation to three of the five illustrated in Fig. 9 *b* of Reedy and Reedy (1985). (*a*) View corresponding to an axial tilt of −25°. In this orientation of the plane of the lead bridge triangle is best presented. At the rear bridge, the view direction is down the midsegment which gives rise to pronounced center beading at the rear bridge in projection (see Fig. 8). (*b*) Untilted orientation in which neither center beading nor straddle beading is developed. (*c*) View oriented at an axial tilt of +25°. This view projects nearly down the lead bridge triangle giving rise to straddle beading. Note the varying degree to which the rear bridge density merges into the lead bridge density.

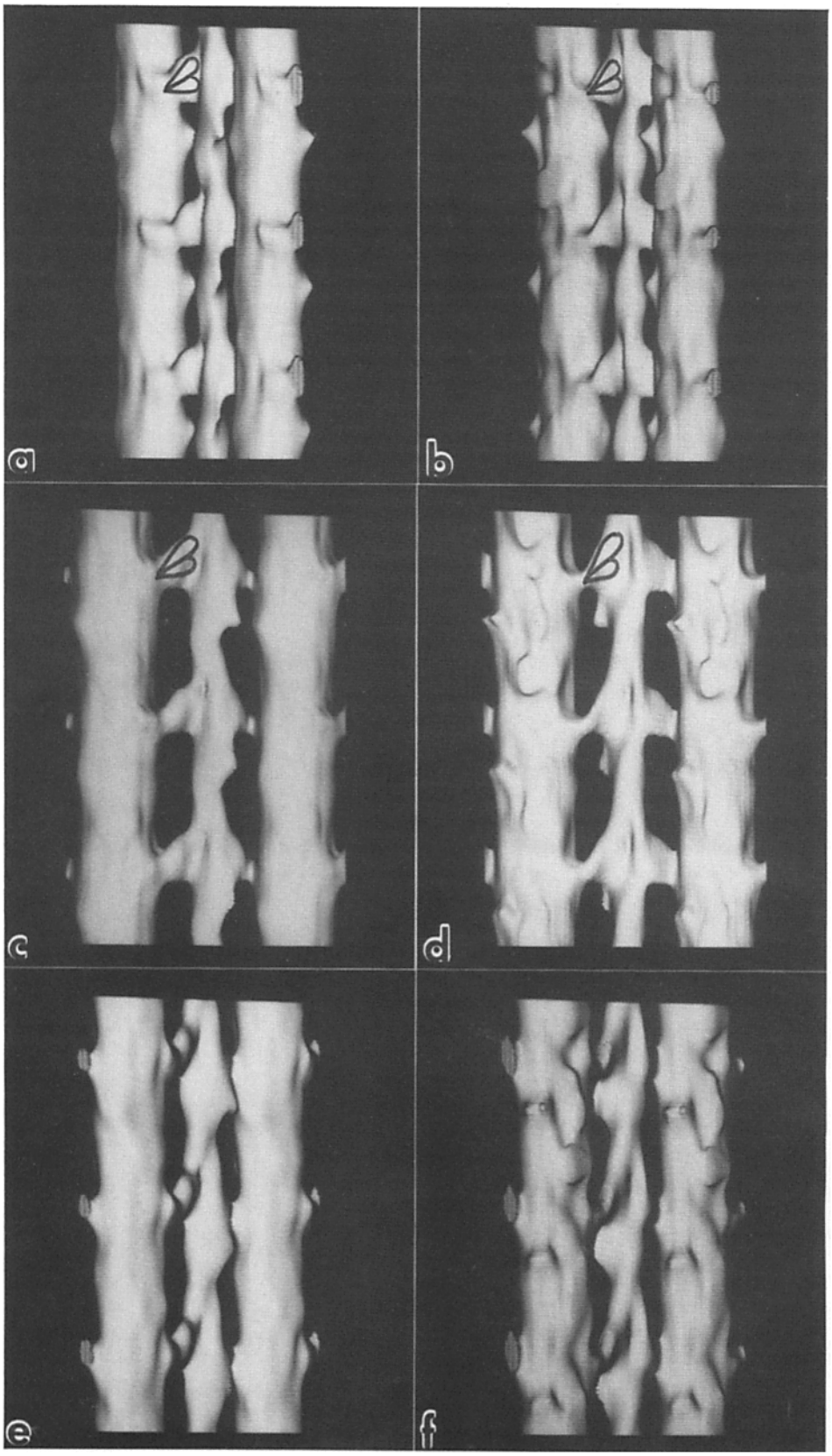

Figure 7. Surface representations of front and back sides of myac layer. These are calculated at a higher density cutoff than those shown in Fig. 6. As a result the rear bridges are not displayed. Panels on the left are front-side views as shown in Fig. 6; panels on the right are back-side views. (*a*) −45°, (*b*) +135°; (*c*) 0°; (*d*) +180°; (*e*) +45°; (*f*) +225°. The suggested position of the two myosin heads in the lead bridge are sketched in *a–d*.

at the head junction observed in rotary shadowed (Elliott and Offer, 1978), unstained (Walzthony et al., 1984), or negatively stained myosin molecules (Walker et al., 1985). An additional region of flexibility nearer to actin is implied by the differing angle of contact between the bridge neck and midsegment of lead and rear bridges.

The thick filament shaft along the gap between double chevrons (interdoublet gap) is featureless and shows no evidence of the 20% of myosin heads believed to be unbound to actin in rigor (Lovell et al., 1981; Goody et al., 1985). On the thick filament at the surface of the reconstruction are the origins of cross-bridges that have been removed by the microtomy process (Fig. 6). Together with the double chevrons they define the left-handed helical path of the actin target lattice (Reedy, 1968). At the level of the lead bridge is a rear bridge stump; at the level of the rear bridge is a lead bridge stump. At the level of the interdoublet gap is a broad disk-like plateau that represents residual mass from a flared-X origin. Features that could be identified with the 14.5-nm-thick filament period are not observed, in agreement with the earlier reconstruction (Taylor et al., 1984).

Projections of the 3-D Reconstruction Compared with Tilted Myac Layers

The approximate 3-D structure of rigor cross-bridges in IFM was deduced by Reedy and Reedy (1985) from studies of tilt views of myac, actin, and flared-X layers. To facilitate comparison with that work, we calculated projection maps and matched surface views of the 3-D reconstruction at the same tilt orientation as original and optically filtered images reported in the earlier work. Although some filtered images in Reedy and Reedy (1985) included unsampled 5.9- and 5.1-nm-thin filament-based layer lines, the corresponding data could not be included in the 3-D reconstruction and so is missing from its projections.

Axial tilts produce characteristic changes in the appearance of myac layers (Reedy and Reedy, 1985). Two patterns develop, one in which the projected cross-bridge density appears as a single dense bead over the thin filament, referred to as "center beading," and the other in which the cross-bridges appear as a pair of dense beads straddling the thin filament, separated by ~8.0–8.5 nm, referred to as "straddle beading." Center and straddle beading arise due to the sigmoidal shape of the cross-bridge–actin complex. Center beading develops in axial tilts when the projection direction is down the midsegment axis of the cross-bridge pair. Straddle beading develops when the projection is down the long axis of the neck-stem.

In projection, center and straddle beading are not prominent in untilted myac layers due to the fact that midsegment and neck-stem are not appropriately oriented to maximize buildup of density in the image. When myac layers are tilted about the filament axis by +25°, straddle beading becomes pronounced at the lead bridge (see Figs. 7 and 9 *a* in Reedy and Reedy, 1985). This appearance is well duplicated from the 3-D reconstruction which has dense elongated and slanted straddle beads at the lead bridges in the simulated +25° axial tilt (Fig. 8 *e*). In the surface display (Fig. 6 *c*), the neck-stem of the lead bridge lies along the direction of view which maximizes density buildup in projection. The 20° rotation of the neck-stem results in slanting of the straddle beads relative to the filament axis. In the same +25° projection map at the rear bridge (Fig. 8 *e*), only a diffuse central bead is found with little density extending toward thick filaments. In the corresponding surface image at the rear bridge (Fig. 6 *c*), the midsegment is angled off the projection direction which is now perpendicular to the neck-stem axis. In this orientation, the mass is spread out and the projected density is low.

Straddle beading, by definition, implies that the density between the beads is low. Both original and filtered images as well as projections of the 3-D map show a line of low density on the thin filament axis separating the two beads of the lead bridge. The presence of this gap is suggestive of separation between the two strands of the thin filament. That suggestion appeared to be supported by the earlier tilt series reconstruction (Taylor et al., 1984) which had a gap between

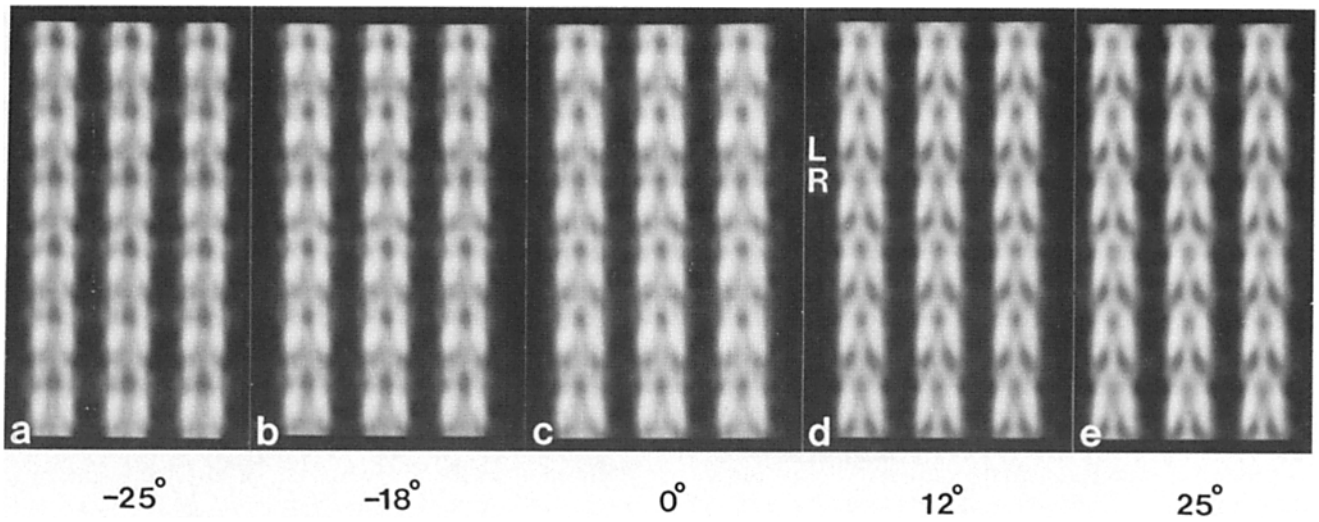

Figure 8. Selected projections of the myac layer 3-D reconstruction. These five projections are identical in orientation to the filtered images shown in Fig. 9 *b* of Reedy and Reedy (1985). They illustrate the development of center beading and straddle beading in axial tilts of myac layers. Lead and rear bridges are labeled *L* and *R*, respectively. View oriented at an axial tilt of (*a*) −25°, (*b*) −18°, (*c*) untilted orientation, (*d*) +12°, and (*e*) +25°. Three inter-thick filament repeats and two axial 116-nm repeats are shown.

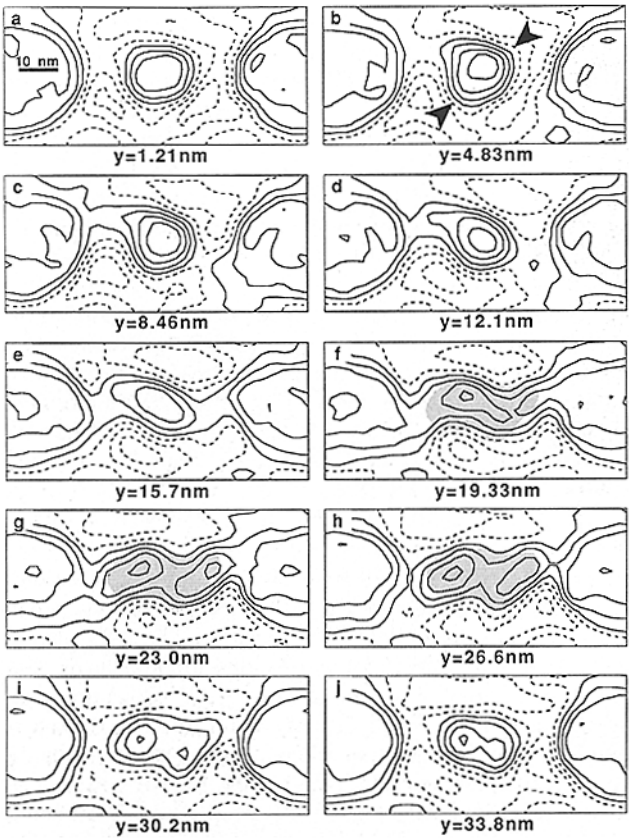

Figure 9. Contoured transverse sections through a double chevron. These maps sample different levels through the first double chevron shown in Fig. 5. *c* and *d* are from the rear bridge region; *f–i* are from the lead bridge region. Superimposed on the contour maps in panels *f–h* is a grey area which represents approximately the size of the midsegment of the cross-bridge seen in *i*. *f–i* illustrate the lack of rotation of the midsegment which should occur if F actin is uniformly twisted in this region. The first and last panels are from the interdoublet gap. Arrowheads in *b* indicate asymmetry in the thin filament profile which is not due to cross-bridges. This may be troponin. These maps are not compensated for section thinning.

the axial actin strands. However, the projected density on the thin filament axis (Fig. 8, *d* and *e*) is actually higher than that through uninterrupted embedding medium. Moreover, the present 3-D map has relatively high density though the center of the thin filament (Fig. 9) thereby suggesting that the actin strands have maintained contact. Therefore the low density between straddle beads in projection images arises largely because of the relatively higher projected density of the neck-stems of the cross-bridge and does not require separation of the actin strands.

Tilting myac layers by −25° about the filament axis converts the diffuse central bead of the rear bridge to a strong dense bead showing weak but distinct connections to the thick filaments (Fig. 8 *a*). The corresponding surface view (Fig. 6 *a*) shows the axis of the rear midsegment oriented along the view direction. In the projection image the lead chevron density becomes diffuse and uniform (Fig. 8 *a*). Surface displays in this view (Fig. 6 *a*) show the triangular shape of the lead bridge to best advantage.

It is not possible to see the interconversion of straddle beading into center beading in myac layers because of tilt angle restrictions in the electron microscope and superposition with the thick filament. In actin layers (Reedy and Reedy, 1985; Taylor et al., 1989) this interconversion can be observed. The agreement between optically filtered images and the projections of the 3-D reconstruction reinforce the validity of both approaches.

Thin Filament Structure

Lead and rear cross-bridges are also associated with local alterations in the helical twist of the thin filament within each 38.7-nm helical repeat. At radii >8 nm from the thin filament axis, the cross-bridge density through lead and rear bridges appears to follow a helical path. At radii <8 nm, a value that encompasses the midsegment of the cross-bridge–actin complex, the densities at the lead bridge run nearly parallel with the filament axis. This effect can be visualized in several ways.

One way is by examination of contoured sections through the lead chevron. The thin filaments of *Lethocerus* have 28 subunits in 13 turns of the 5.9-nm left-handed genetic helix (Miller and Tregear, 1972). In a uniformly twisted thin filament we would expect a rotation of 26° per actin monomer along each strand, corresponding to an axial translation of 5.5 nm. Each of the two lead bridges of the chevron extend ~15 nm axially in the map and by virtue of their size should encompass two actin monomers each. In contoured sections through the lead chevron (Fig. 9), the midsegment does not rotate over this distance. Instead, the length of the midsegment increases in concert with shortening of the neck-stem, as sections proceed from the M line side towards the Z line.

In our first reconstruction, we quantitated the degree of thin filament twist by plotting the azimuth and radius of cylindrical densities believed to represent actin strands (Taylor et al., 1984). In the present reconstruction actin cannot be resolved from the cross-bridges. To obtain a quantitative estimate of the filament twist in the present reconstruction, we cross-correlated an acto-S1 helical projection (Taylor and Amos, 1981) with sections from the 3-D reconstruction calculated transverse to the thin filament axis. This procedure used the fact that the helical projection has an outline similar to that of the cross-bridges and is based on the premise that the asymmetry in the thin filament profile is due to cross-bridge mass. The presence of other structures, such as troponin, violate this premise and may make the plot of rotation angle with axial coordinate depart from the actin helix. In addition, no meaningful alignment can be expected where no cross-bridge mass projects from the thin filament. In this analysis only rotation angle was searched because the myac layer reconstruction was prealigned with the presumptive twofold rotation axes of its filaments. Helical projections of acto-S1 were calculated using just the 2nd layer line, 2nd and 4th layer lines and 2nd, 4th, and 6th layer lines, and with and without equators to probe the sensitivity of the rotational alignment to the motif shape. The analysis was also carried out using myac layer thin filaments stretched along Z* by differing extents to compensate for section thinning. The correlation coefficient was sensitive to (*a*) the amount of stretch in Z applied to the myac layer, (*b*) the inclusion of equatorial data in the helical projection, and (*c*) inclusion of higher order layer lines in the helical projection. However, the shape of the rotation curve was much less sensitive to these factors. The results shown (Fig. 10) are typical.

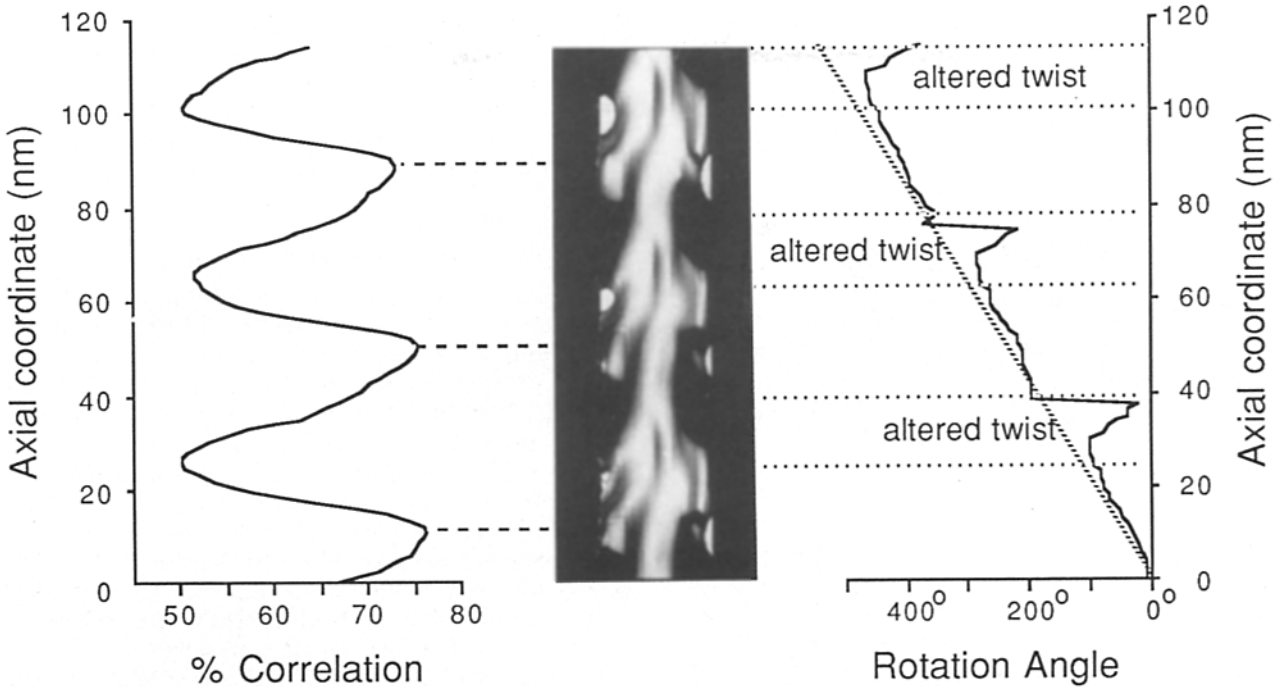

Figure 10. Plots of rotational alignment of the acto-S1 helical projection with the myac layer thin filament. The graph on the left is the correlation coefficient at the angle of rotation for best alignment of the helical projection with each section of the myac layer (sampled axially in 1.21-nm steps). The graph on the right shows the angle of rotation for the helical projection where the best alignment with the individual myac layer section occurs. This graph would be linear with a slope of 4.66°/nm for a regular 28/13 helix. Abrupt discontinuities occur at the ends of the angular search range (0°–180°); at these points an additional 180° was added to the calculated angle to align the linear parts of the curve for successive double chevrons with the predicted curve (shown as a dashed line). Apparent left handed twist represents a rotational jump of the helical projection motif to the opposite long pitch helical track. The surface display in the center relates the structural features to the respective regions of the graphs.

The curves obtained generally had three regions of different twist within each 38.7 nm repeat: (*a*) through the rear bridge, the rotation followed that predicted for the 28/13 helix of the thin filament, (*b*) at the lead bridge, the rotation curve flattened out indicating a region of little or no filament twist, and (*c*) in the interdoublet gap between successive double chevrons the graph appeared to show reversed twist (left handed). The correlation coefficients varied through the bridging regions. They were highest at the rear bridge. They were lowest in the region of the trailing head of the lead bridge, indicating that the crossbridge structure differs most from acto-S1 at that position.

The apparent reversed twist in the interdoublet gap is unlikely to be a significant indicator of F actin twist. It represents instead a rotational jump in the alignment of the helical projection motif from one actin long pitch helical track to the other. The rotational correlation calculation is measuring asymmetry in the thin filament profile which arises from either cross-bridge or troponin mass. In the interdoublet gap the thin filament profile has little asymmetry with which to define the long pitch helix. Thus, as sections of the 3-D map approach the next bridging level through the interdoublet gap, the location of the long pitch helices is determined by the little residual asymmetry present in the unlabeled thin filament profile. This residual asymmetry may be insufficient to detect the long pitch helices in the presence of other features. The rotation of the motif could then get out of alignment with the long pitch helix enough to shift to the wrong track upon reaching the region of pronounced asymmetry associated with the next double chevron level. In fact a minor asymmetry is detectable in the interdoublet gap in a position believed to be occupied by troponin. The asymmetry is subtle (Figs. 9, *a–d*) but is clearly out of azimuthal alignment with the cross-bridge density.

An additional perspective on these nonuniformities in the thin filament structure can be obtained from cylindrical sections calculated about the thin filament axis (Fig. 11). At a radius of 7.0 nm, a distance well outside of the thin filament envelope, cylindrical sections show three pairs of wedge-shaped features per 116 nm, representing the three pairs of double chevrons. The widest part of each wedge occurs on the M-line side of the chevrons, the narrowest point on the Z-line side. Contours at the left-hand side of each wedge appear to run generally vertically, whereas the contours on the right-hand side follow approximately the tracks of the long-pitch actin helix. At 9.5-nm radius and higher, the densities follow the expected helical path. The cylindrical sections also illustrate the relative sizes of lead and rear bridges compared with S1, supporting the interpretation that they are double- and single-headed cross-bridges, respectively.

These indications of local variation in twist are not simply artifacts of the low resolution of reconstruction. Both the correlation analysis and the cylindrical sections show that twist of the expected magnitude can be observed through the rear bridge region of the map, a distance that is comparable to that through the untwisted region of the lead bridge.

At this resolution, the thin filament is expected to contain density modulations due to troponin as well as cross-bridges.

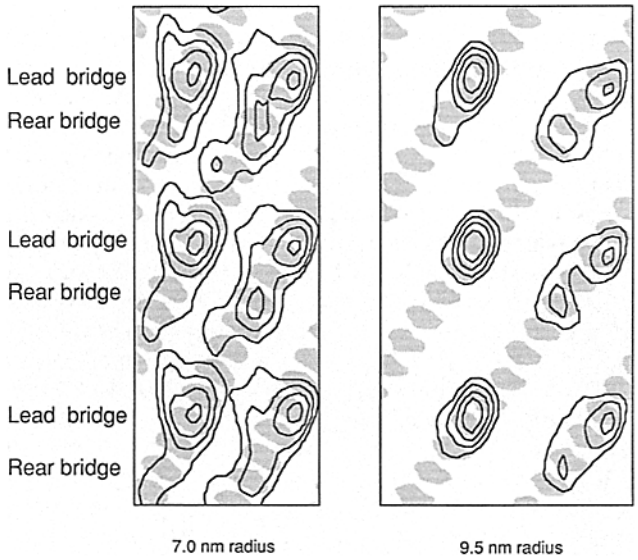

Figure 11. Plots of cylindrical sections about the myac layer thin filament at radii of 7.0 and 9.5 nm. Solid lines are the myac layer contours starting with the same cutoff used for the surface images of Fig. 6. For the cylindrical section calculation, the myac layer reconstruction was stretched by a factor of 1.4 normal to the section plane to compensate for section thinning. Shaded areas are cylindrical sections calculated through an acto-S1 reconstruction (Taylor and Amos, 1981) which illustrate both the relative sizes of S1 with respect to lead and rear bridges and the behavior of a regular 28/13 helix. The maps show a full 116-nm axial period and have been scaled in the horizontal direction to give the correct circumference.

The heavy troponin species in *Lethocerus* is staggered on adjacent thin filaments (Reedy, M. C., B. Bullard, and M. K. Reedy, unpublished observations) in contrast to the laterally in-register arrangment of vertebrate muscle (Ohtsuki, 1975). This staggered arrangement makes troponin congruent with the pattern of rigor cross-bridge attachments (Wray et al., 1978) so that troponin mass could be partly merged with cross-bridge detail. This may account for the lack of any clearly separated feature that we can suggest as troponin.

Comparison of Symmetrized and Unsymmetrized Reconstructions

There are no significant differences between the reconstruction illustrated here and done in p1 and the earlier reconstruction done in p12 (see Taylor et al., 1986), which enforced twofold rotation symmetry about the filament axes. Small differences in density and shape between bridges on opposite sides of the filament axis present in p12 were lost as were some features which probably represent noise. However, the major features of the reconstruction, namely the triangular shape of the lead bridge, the relatively lower size, density, and tilt of the rear bridges and the apparent local changes in the actin filament helical structure are invariant with respect to symmetrization.

Discussion

Three-dimensional reconstructions of IFM provide detailed information on cross-bridge structure in situ that contrasts with the picture of uniform myosin heads obtained from in vitro studies of acto-S1. The present 3-D reconstruction improves on that reported earlier (Taylor et al., 1984) because addition of myac row and column data results in more complete measurement of the myac layer transform and corrects to a large extent the effects of the missing cone. The conclusions about rigor cross-bridge structure drawn from the earlier work gain support and additional detail from this reconstruction.

Rigor Cross-Bridges Have Different Structures

The myac layer reconstruction from tilt series data alone (Taylor et al., 1984) revealed two cross-bridge classes that differ in tilt, density, and slew. The dense lead bridges were tilted at 45° and bent backward against the slew curvature seen in acto-S1. The less dense rear bridges were barely tilted and had conventional S1 slew curvature. The axial dimensions of both cross-bridges were the same although the rear bridge was much less dense than the lead. From these observations we concluded that lead bridges were composed of two tilted myosin heads bound to successive actin monomers on one thin filament and that the rear bridges consisted of a single, nearly untilted myosin head, delocalized in the averaged reconstruction over two actin monomers.

The new reconstructions reinforce the case for two-headed lead bridges and single-headed rear bridges. Rear bridges remain low density features but are now confined to a smaller volume in isodensity contour displays. The smaller size of the rear bridge is a direct result of the addition of myac column and myac row data which define the density profile across the section along the Z axis. When information on the density profile is absent, the contour level that represents the interface between protein and embedding media varies with distance from the central plane of the reconstruction (Amos et al., 1982). The inclusion in the reconstruction of transform data from three orthogonal views resolves the problem of contour interface which resulted in enlarged features at the surface of the earlier reconstruction that particularly affected the size of the rear bridges.

In the present reconstruction lead bridges show a distinctly triangular shape. In this triangle the edge closest to the Z line is aligned perpendicular to the filament axis, while the edge closest to the M line is tilted at ~45°. One vertex forms the cross-bridge origin on the thick filament. Despite the fact that individual myosin heads cannot be resolved in the lead bridge, its shape must be a manifestation of myosin head conformation. Thus, the front edge of this cross-bridge has a slope consistent with that expected for 45° myosin heads but the 90° orientation of the trailing edge of the lead bridge cannot be explained by a 45° tilted head. The triangular shape of the rigor lead bridge is also observed in (*a*) the 3-D reconstruction of the rigor actin layer (Taylor et al., 1989), (*b*) oblique section reconstructions of 15-nm cross-sections (Taylor, K. A., M. C. Reedy, M. K. Reedy, and R. A. Crowther, unpublished observations), (*c*) cross-bridge structures observed in swollen rigor IFM fibers (Reedy et al., 1988).

The triangular shape of the lead bridge must result from several possible arrangements of myosin heads which differ in the origin and number of myosin heads in each cross-bridge. Two models for myosin head distribution within cross-bridges in muscle are relevant to this issue.

The model of Offer and Elliott (1978) deals primarily with head distribution in *Lethocerus*. Their model proposes that each head of a myosin molecule binds to a separate thin fila-

ment (two-filament binding), forming a single-headed lead bridge on one filament and a single-headed rear bridge on the adjacent thin filament. A single myosin head delocalized in the averaged reconstruction over two actin monomers might account for the shape of the averaged lead bridge if the individual heads were distributed over 90° and 45° orientations. However, this arrangement is not consistent with the high average density of the lead bridge. In addition, exclusive formation of single-headed cross-bridges would account for only 56% of the myosin heads (Offer et al., 1981), whereas several lines of evidence indicate that ~80% of the myosin heads are bound to actin in rigor IFM (Lovell et al., 1981; Goody et al., 1985). Therefore, it seems unlikely that the triangular shape arises from single-headed bridges.

Another major model (Squire, 1972) commonly used to describe vertebrate muscles, proposes that both heads of one myosin bind to the same thin filament; therefore, most, or all, cross-bridges contain both heads of one myosin molecule, and nearly all myosin heads are bound in rigor. This model would produce the triangular shape of the lead bridge, but the small size of the rear bridge and the general agreement that a significant portion of myosin heads are not bound in IFM rigor argue against this model's applicability to cross-bridges in *Lethocerus*.

A third model would combine a mixture of single- and two-filament interactions and both single- and double-headed cross-bridges. In this mixed model, double-headed bridges would contain myosin heads from different myosin molecules. The mixed model could achieve ~75–80% actin-bound heads by using strict two-filament interactions for 9/16 of the myosin molecules, each providing one head to a lead bridge and one to a rear bridge. The additional heads for lead bridges, needed to account for their larger size, would be drawn from the remaining 7/16 of myosin molecules, binding single-headed thus constituting each lead bridge from myosin heads of two different myosin molecules. (Note that 9/16 leaves only 7/16 of the myosin molecules [14] to contribute one extra head to each of the 18 lead bridges in each 116-nm axial repeat.) This model would result in a more reasonable number of actin-bound heads (78%) but also has some unpleasant consequences.

Offer et al. (1981) showed how exclusive two-filament interactions could produce the observed lattice of flared X's while requiring minimal departures from the surface lattice of myosin origins. The mixed model would violate this consideration by requiring large departures from the myosin surface lattice to place an additional head from a second myosin molecule into the lead bridge, and to place the vertices of these two myosin molecules in close proximity. The latter is necessary to produce the observed appearance of a common origin on the thick filament, in keeping with the two-strandedness of flared-X cross sections (Reedy and Reedy, 1985). In addition, this mixed model predicts that variations in density and bridge distribution of double chevrons, which are the major expression of the 116-nm period (Reedy and Garrett, 1977), would arise from lead chevron variations (because 2/9 of lead chevrons would remain single-headed), when in fact, original images and 3-D reconstructions demonstrate such variations most obviously in rear chevrons. We think it unlikely that half of the myosins would form cross-bridges with minimal circumferential and axial movements (two-filament binding) while the myosins involved in single-filament interactions were forced into large departures from their origins on the thick filament surface lattice. In fact, such departures from the resting surface lattice in rigor would contradict the fundamental premise of the two-filament binding proposal (Offer and Elliott, 1978).

We propose that rigor cross-bridges in *Lethocerus* arise from single-filament interactions. If 80% of the myosin heads in *Lethocerus* are attached to actin in rigor, and only single-filament interactions occur, it follows that some of the bridges must be double-headed and some single-headed. We suggest that steric factors (limits on head flexibility, local actin twist variations, troponin size, and placement) prevent the second head from binding in the rear bridge. We propose that the triangular shape of the lead bridges results when both heads from one myosin molecule bind along a single thin filament.

Our conclusion that the triangular shape represents a two-headed myosin molecule is supported by higher resolution views of two-headed binding by myosin molecules to single thin filaments observed in negatively stained preparations of acto-HMM (Craig et al., 1980) and crayfish fast muscle (Bard et al., 1987). It is important to note that because the two heads in the triangular lead bridge originate from a common vertex but bind to different actin subunits, each head must have a different conformation. In particular, they differ in tilt angle. Moreover, further distinctions between the two heads relate to local alterations in the helical structure of actin.

Helical Structure of Actin

Features of the myac reconstruction from tilt series data alone suggested that regular variations in the helical structure of the thin filament were associated with bridge attachment. Strands of density running axially in the reconstruction were interpreted as the long pitch helical strands of the thin filament. In the rear bridge region these actin strands appeared to have greater than normal twist but normal spacing. In the lead bridge region the strands appeared to be untwisted and separated. We considered that the twist variations express plausible strain differences between one-headed and two-headed bridge attachments, but considered the strand separation more likely to be an artifact of fixation-embedding. We further noted the position of the strands relative to the lead bridge suggested a binding geometry in agreement with that proposed by Taylor and Amos (1981) and contrary to that proposed by Moore et al. (1970). These interpretations require some modification in light of the present reconstruction.

After addition of thick section data, the reconstruction does not separate the long pitch helical strands of actin from cross-bridge features, although there are density peaks within the lead chevron positioned at similar radii to the long pitch helical strands observed in the earlier reconstruction. It now seems more likely that the densities identified earlier as actin are derived from both cross-bridges and actin. The addition of cross-bridge mass to actin at high radius, in effect produces an outward shift in the center of mass of these axial densities. Because we cannot separate actin from myosin head, the reconstruction cannot convincingly address the question of binding geometry between myosin and actin, whether of the Taylor and Amos or any other type.

The present reconstruction, however, resolves the problem

of the gap between the axial strands observed in the earlier work. Instead of a gap between the two actin strands at the lead bridge, the density is uninterrupted through the thin filament. Optically filtered images of myac layers at tilt angles that produce straddle beading, present a low density gap on the thin filament axis (Reedy and Reedy, 1985). The calculated projections of the present reconstruction also show this gap, despite the density continuity through the thin filament. Thus, filtered projections and original images that suggest a gap between actin strands in regions having bound cross-bridges are not evidence of strand separation. Instead, this gap is an illusion arising from contrast with the considerably higher projected density of the cross-bridges relative to the thin filament axis. The strength of this straddle beading is such that it dominated the 3-D reconstruction from tilt series data alone, because the equatorial data, which provide the radial density profiles of the filaments, was incomplete. The addition of myac row data completes the equatorial data and produces a more realistic density map.

Local, periodic departures from uniform helical twist of the thin filament are still indicated after the addition of thick section data. This conclusion is based on the premise that the cross-bridge density should reflect the helical structure of the underlying thin filament and that the relationship between myosin and actin is identical for all bound heads. In the present reconstruction these twist alterations are manifest in (*a*) midsegment rotation, (*b*) rotational cross-correlations with acto-S1 motifs, and (*c*) cylindrical sections. Through the lead bridge region, the thin filament appears untwisted; apparently normal twist for a 28/13 actin helix is observed through the rear bridge region, and by inference, there should be greater than normal twist through the interdoublet gap such that the 38.7-nm crossover repeat is preserved. These variations differ in one important respect from the earlier reconstruction (Taylor et al., 1984) which assigned overtwist to the rear bridge rather than to the interdoublet gap.

The observed rotation of the lead bridge triangle, mentioned earlier, could be a natural consequence of thin filament untwisting. Let us assume that the two actin monomers that form the termination points of the two myosin heads in the lead bridge are separated axially by 5.5 nm with no rotation in the untwisted filament. If the two myosin heads originate from a common vertex within the same molecule and have the same length, and the forward head is tilted to form the 45° angled edge of the triangle, the less angled trailing head must bend to fit its length into the shorter path from thick filament origin to actin terminus. This rotates the triangle and places the trailing edge closer to the thick filament surface than the forward edge (Fig. 12). Paradoxically, this arrangement makes the portions of the lead bridge distal to the thin filament appear helical while the portions near the thin filament do not. More importantly it suggests that the conformational differences between the heads in the lead bridge include variations in bending as well as tilt angle.

The apparent lack of twist through the lead bridge may have alternate interpretations. In the strictest sense, what we observe here is lack of rotation of the midsegment of the lead bridge which contains both actin and the actin binding domain of the myosin head. The lack of clear definition of the thin filament boundary within the bridging region leaves open several possible arrangements of actin monomers with respect to the myosin heads. A possibility that cannot be

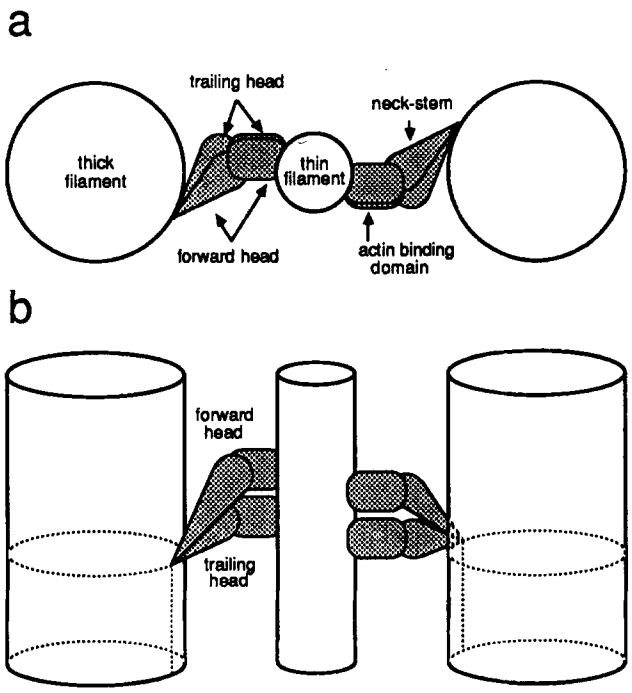

Figure 12. Schematic diagram of the arrangement of myosin heads proposed for the lead bridge. (*a*) View down the filament axis. Cross-bridges bind to actin approximately along the inter-thick filament axis. Actin-binding domains of the two myosin heads within one lead bridge are positioned along successive actin monomers without rotation while myosin heads in the two lead bridges of the chevron are positioned opposite each other. Neck-stem domains connect actin-binding domains to the thick filament but must be positioned differently at the forward and trailing heads to accommodate the similar length into differing distances from the common vertex to the actin binding domain. The midsegment of the chevron includes the thin filament and actin-binding domains of opposed cross-bridges and morphologically would also include any neck-stem mass that aligned with the long axis of the midsegment. The positioning of the neck–stem relative to actin binding domain at the trailing head thus gives its midsegment greater length than the midsegment of the forward head. (*b*) Longitudinal view that shows how two heads at differing tilt angle can give rise to a triangular-shaped cross-bridge at low resolution.

completely ruled out at this time is a contribution of the large troponin complex to the structure of the lead bridge. However, anti–troponin monoclonal antibodies have detected troponin epitopes at the rear bridge rather than the lead bridge (Reedy, M. C., and B. Bullard, unpublished observations).

Our preferred interpretation is that the actin filament is untwisted in the lead bridge region. This is consistent with observations of torsional flexibility in actin filaments by electron microscopy (Egelman et al., 1982, 1983; Stokes and DeRosier, 1987) and by optical measurements (Thomas et al., 1979; Yoshimura et al., 1984). In this scheme, the inevitable distortion engendered by the binding of two heads of one myosin successively along the same actin strand is partly expressed by the local untwisting of actin to accommodate a fixed relationship between actin and the binding domain of the myosin head. However, this local untwisting of the actin filament may require a distortion considerably greater than that observed in other structures.

It is possible that the actin filament may retain normal twist within the midsegment of the lead bridge. If so, this would

require the conformation of the myosin heads to conceal the helical twist of actin and seems to require two different acto-myosin binding geometries in the lead bridge. It is also conceivable that the two-domain actin monomer itself (Kabsch et al., 1985) may absorb any distortion, allowing the filament to remain normally twisted while acto-myosin binding geometry remains constant. This requires that the link between actin domains be flexible and that rigor cross-bridges bind to only one actin domain, to allow this flexibility to express itself.

Not all these possible interpretations seem equally likely. As Goody and Holmes (1983) have pointed out, it is difficult to imagine how the strong, but noncovalent, bond in rigor or during the power stroke could result from interaction between actin and myosin at any one of several different stereospecific binding sites. We think it more likely that the interface between actin and myosin is the same for all rigor heads, and that combinations of filament untwisting and differing myosin head conformation could accommodate the distortion arising from single-filament binding of two-headed bridges.

Summary

The present reconstruction of the myac layer resolves several questions relating to features observed in the earlier work. The importance of complementing tilt views with additional projections outside of the tilt range of the microscope goniometer is clearly evident from comparison with the earlier myac layer reconstruction. The changes in the reconstruction resulting from incorporation of this additional data include (*a*) better density continuity through the lead chevron and a better density profile for the thin filament, (*b*) a clarification of the triangular shape of the lead bridges, (*c*) a smaller size for the rear bridges. Despite these changes three conclusions drawn from the earlier work are substantiated: (*a*) two forms of in situ rigor cross-bridges are observed which differ with respect to tilt, size, density, and slew; (*b*) rigor cross-bridges may contain on average either one or two myosin heads, that bind along a single thin filament; (*c*) local perturbations are observed in the expected smoothly helical structure of the myosin head-actin complex.

The major observation of this reconstruction is that rigor cross-bridges can have different conformations and that the individual heads of double-headed rigor cross-bridges may also have different conformations. To achieve this, multiple domains, flexibly connected must be present in each myosin head. At least one of these must occur at the head vertex to allow for both tangential and radial variations in cross-bridge origins. Another seems necessary near the junction of neck-stem with midsegment where its flexibility is expressed in the differing tilt angles of the cross-bridges and in the kink of the trailing head of the lead bridge. Conceivably the rear bridge may duplicate the midsegment configuration of the trailing head of the lead bridge, implying only two different head conformations. If not, then our reconstruction implies three different head conformations in rigor. In either case, our reconstruction supports the idea that there are different conformational states of myosin heads in the strongly bound state. To what extent these differences are due to spatial positioning within the filament lattice or to temporal events in the rigor power stroke remains to be determined.

We thank the MRC Laboratory of Molecular Biology for use of their scanning densitometer, Ms. Vivian Fowler for typing the manuscript, and Ms. Suzanne Goodman for technical assistance.

This research supported by National Institutes of Health grants GM 30598, AM 14317, and grants from the Muscular Dystrophy Association. The PDS scanner was purchased from funds supplied by National Institutes of Health grant RR02283 and NSF grant PCM 8400167. K. A. Taylor is an Established Investigator of the American Heart Association.

Received for publication 2 December 1988 and in revised form 12 May 1989.

References

Amos, L. A. 1985. Structure of muscle filaments studied by electron microscopy. *Annu. Rev. Biophys. Biophys. Chem.* 14:291–313.

Amos, L. A., and T. S. Baker. 1979. Three-dimensional image of tubulin in zinc-induced sheets, reconstructed from electron micrographs. *Int. J. Biol. Macromol.* 1:146–156.

Amos, L. A., R. Henderson, and P. N. T. Unwin. 1982. Three-dimensional structure determination by electron microscopy of two-dimensional crystals. *Prog. Biophys. Mol. Biol.* 39:183–231.

Bard, F., C. Franzini-Armstrong, and W. Ip. 1987. Rigor crossbridges are double headed in fast muscle from crayfish. *J. Cell Biol.* 105:2225–2234.

Baumeister, W., M. Barth, R. Hegerl, R. Guckenberger, M. Hahn, and W. O. Saxton. 1986. Three-dimensional structure of the regular surface layer (HPI layer) of *Deinococcus radiodurans*. *J. Mol. Biol.* 187:241–253.

Bennett, P. M. 1974. Decrease in section thickness on exposure to the electron beam; the use of tilted section in estimating the amount of shrinkage. *J. Cell Sci.* 15:693–701.

Berriman, J., and K. R. Leonard. 1986. Methods for specimen thickness determination in electron microscopy II. Changes in thickness with dose. *Ultramicroscopy.* 19:349–366.

Bullard, B., K. Leonard, A. Larkins, G. Butcher, C. Karlik, and E. Fyrgerg. 1988. Troponin of asynchronous flight muscle. *J. Mol. Biol.* 204:621–637.

Craig, R., A. G. Szent-Gyorgyi, L. Beese, P. Flicker, P. Vibert, and C. Cohen. 1980. Electron microscopy of thin filaments decorated with a Ca^{++}-regulated myosin. *J. Mol. Biol.* 140:35–55.

Egelman, E. H., N. Francis, and D. J. DeRosier. 1982. F-actin is a helix with a random variable twist. *Nature (Lond.).* 298:131–135.

Egelman, E. H., N. Francis, and D. J. DeRosier. 1983. Helical disorder and the filament structure of F-actin are elucidated by the angle-layered aggregate. *J. Mol. Biol.* 166:605–629.

Egerton, R. F. 1980. Measurement of radiation damage by electron energy-loss spectroscopy. *J. Microsc.* 118:389–399.

Elliott, A., and G. Offer. 1978. Shape and flexibility of the myosin molecule. *J. Mol. Biol.* 123:505–519.

Goody, R. S., and K. C. Holmes. 1983. Cross-bridges and the mechanism of muscle contraction. *Biochem. Biophys. Acta.* 726:13–39.

Goody, R. S., M. C. Reedy, W. Hofmann, K. C. Holmes, and M. K. Reedy. 1985. Binding of myosin subfragment 1 to glycerinated insect flight muscle in the rigor state. *Biophys. J.* 47:151–169.

Holmes, K. C., R. T. Tregear, and J. Barrington-Leigh. 1980. Interpretation of the low angle X-ray diffraction from insect flight muscle in rigor. *Proc. R. Soc. Lond. B Biol. Sci.* 207:13–33.

Holser, W. T. 1958. Point groups and plane groups in a two-sided plane and their subgroups. *Z. Kristallogr.* 110:226–281.

Huxley, A. F. 1957. Muscle structure and theories of contraction. *Prog. Biophys. Chem.* 7:255–318.

Huxley, A. F., and R. Niedergerke. 1954. Interference microscopy of living muscle fibres. *Nature (Lond.).* 173:971–973.

Huxley, H. E. 1969. The mechanism of muscular contraction. *Science (Wash. DC).* 164:1356–1366.

Huxley, H., and J. Hanson. 1954. Changes in the cross-striations of muscle during contraction and stretch and their structural interpretation. *Nature (Lond.).* 173:973–976.

Kabsch, W., H. G. Mannherz, and D. Suck. 1985. Three dimensional structure of the complex of actin and DNase I at 4.5Å resolution. *EMBO (Eur. Mol. Biol. Organ.) J.* 4:2113–2118.

Kensler, R. W., and M. Stewart. 1983. Frog skeletal muscle thick filaments are three-stranded. *J. Cell Biol.* 96:1797–1802.

Lamvik, M. K. 1978. Muscle thick filament mass measured by electron scattering. *J. Mol. Biol.* 122:55–68.

Lovell, S. J., P. J. Knight, and W. F. Harrington. 1981. Fraction of myosin heads bound to thin filaments in rigor fibrils from insect flight and vertebrate muscles. *Nature (Lond.).* 293:664–666.

Miller, A., and R. T. Tregear. 1972. The structure of insect fibrillar flight muscle in the presence and absence of ATP. *J. Mol. Biol.* 70:85–104.

Milligan, R. A., and P. F. Flicker. 1987. Structural relationships of actin, myosin and tropomyosin revealed by cryo-electron microscopy. *J. Cell Biol.* 105:29–39.

Moore, P. B., H. E. Huxley, and D. J. DeRosier. 1970. Three dimensional

reconstruction of F-actin, thin filaments and decorated thin filaments. *J. Mol. Biol.* 50:279–295.

Offer, G., and A. Elliott. 1978. Can a myosin molecule bind to two actin filaments? *Nature (Lond.).* 271:325–329.

Offer, G., J. Couch, E. O'Brien, and A. Elliott. 1981. Arrangement of cross-bridges in insect flight muscle in rigor. *J. Mol. Biol.* 151:663–702.

Ohtsuki, I. 1975. Distribution of troponin components in the thin filament studied by immunoelectron microscopy. *J. Biochem.* 77:633–639.

Reedy, M. K. 1968. Ultrastructure of insect flight muscle. I. Screw sense and structural grouping in the rigor cross-bridge lattice. *J. Mol. Biol.* 31:155–176.

Reedy, M. K., and M. C. Reedy. 1985. Rigor crossbridge structure in tilted single filament layers and flared-X formations from insect flight muscle. *J. Mol. Biol.* 185:145–176.

Reedy, M. K., and W. E. Garrett. 1977. Electron microscope studies of *Lethocerus* flight muscle in rigor. *In* Insect Flight Muscle. R. T. Tregear, editor. Elsevier Science Publishers, Amsterdam. 115–143.

Reedy, M. K., K. C. Holmes, and R. T. Tregear. 1965. Induced changes in orientation of the cross-bridges of glycerinated insect flight muscle. *Nature (Lond.).* 207:1276–1280.

Reedy, M. K., K. R. Leonard, R. Freeman, and T. Arad. 1981. Thick filament mass determination by electron scattering measurements with the scanning transmission electron microscope. *J. Muscle Res. Cell Motil.* 2:45–64.

Reedy, M. K., R. S. Goody, W. Hofmann, and G. Rosenbaum. 1983. Coordinated electron microscopy and X-ray studies of glycerinated insect flight muscle. I. X-ray diffraction monitoring during preparation for electron microscopy of muscle fibres fixed in rigor, in ATP and in AMPPNP. *J. Muscle Res. Cell Motil.* 4:25–53.

Reedy, M. C., M. K. Reedy, and R. T. Tregear. 1988. Two attached non-rigor crossbridge forms. *In* Molecular Mechanism of Muscle Contraction. H. Sugi and G. H. Pollack, editors. Plenum Publishing Corp., New York. 5–15.

Squire, J. M. 1972. General model of myosin filament structure II. Myosin filaments and crossbridge interactions in vertebrate striated and insect flight muscles. *J. Mol. Biol.* 72:125–138.

Stokes, D. L., and D. J. DeRosier. 1987. The variable twist of actin and its modulation by actin-binding proteins. *J. Cell Biol.* 104:1005–1017.

Taylor, K. A., and L. A. Amos. 1981. A new model for the geometry of the binding of myosin crossbridges to muscle thin filaments. *J. Mol. Biol.* 147:297–324.

Taylor, K. A., M. C. Reedy, L. Córdova, and M. K. Reedy. 1984. Three-dimensional reconstruction of rigor insect flight muscle from tilted thin sections. *Nature (Lond.).* 310:285–291.

Taylor, K. A., M. C. Reedy, L. Córdova, and M. K. Reedy. 1986. Image reconstruction using electron micrographs of insect flight muslce: use of thick transverse sections to supplement data from tilted thin longitudinal sections. *Biophys. J.* 49:353–364.

Taylor, K. A., M. C. Reedy, L. Córdova, and M. K. Reedy. 1989. Three-dimensional image reconstruction of insect flight muscle. II. The rigor actin layer. *J. Cell Biol.* 109:1103–1123.

Thomas, D. D., J. C. Seidel, and J. Gergely. 1979. Rotational dynamics of spin-labeled f-actin in the sub-millisecond time range. *J. Mol. Biol.* 132: 257–273.

Toyoshima, C., and T. Wakabayashi. 1985. Three-dimensional image analysis of the complex of thin filaments and myosin molecules from skeletal muscle. IV. Reconstitution from minimal- and high-dose images of the actin-tropomyosin-myosin subfragment-1 complex. *J. Biochem.* 97:219–243.

Tregear, R. T., and J. M. Squire. 1973. Myosin content and filament structure in smooth and striated muscle. *J. Mol. Biol.* 77:279–290.

Vibert, P., and R. Craig. 1982. Three-dimensional reconstruction of thin filaments decorated with a Ca^{2+}-regulated myosin. *J. Mol. Biol.* 157:299–319.

Vigers, P. A., R. A. Crowther, and B. M. F. Pearse. 1986. Three-dimensional structure of clathrin cages in ice. *EMBO (Eur. Mol. Biol. Organ.) J.* 5:529–534.

Walker, M., P. Knight, and J. Trinick. 1985. Negative staining of myosin molecules. *J. Mol. Biol.* 184:535–542.

Walzthony, D., M. Bahler, H. M. Eppenberger, T. Walliman, and A. Engel. 1984. Unshadowed myosin molecules: STEM mass-maps of myosin heads. *EMBO (Eur. Mol. Biol. Organ.) J.* 3:2621–2626.

Wray, J. S. 1979. Structure of the backbone in myosin filaments of muscle. *Nature (Lond.).* 277:37–40.

Wray, J., P. Vibert, and C. Cohen. 1978. Actin filaments in muscle: pattern of myosin and tropomyosin/troponin attachments. *J. Mol. Biol.* 124:501–521.

Yoshimura, H., T. Nishio, and K. Mihashi. 1984. Torsional motion of eosin-labeled f-actin as detected in time-resolved anisotrophy decay of the probe in the sub-millisecond time range. *J. Mol. Biol.* 179:453–467.